

Ring dark solitary waves: experiment versus theory

A. Dreischuh, D. Neshev

*Sofia University, Department of Quantum Electronics, 5, J. Bourchier Blvd., BG-1164 Sofia, Bulgaria
(Fax.: +3592/9625276, E-mail: ald@phys.uni-sofia.bg)*

G. G. Paulus¹, F. Grasbon¹, H. Walther^{1,2}

¹*Max-Planck-Institut für Quantenoptik, Hans-Kopfermann-Strasse 1, D-85748 Garching, Germany
(Fax.: +4989/329050, E-mail: ggp@mpq.mpg.de)*

²*Ludwig-Maximilians-Universität, Sektion Physik, Am Coulombwall 1, D-85747 Garching, Germany
(Fax.: +4989/2891 4142, E-mail: Prof.H.Walther@mpq.mpg.de)*

(November 5, 2018)

Theoretical and experimental results on optical ring dark solitary waves are presented, emphasizing the interplay between initial dark beam contrast, phase-shift magnitude, background-beam intensity and saturation of the nonlinearity are presented. The results are found to confirm qualitatively the existing analytical theory and are in agreement with the numerical simulations carried out.

PACS:42.65.Tg;42.65.-k;42.65.Jx;42.65.Jv

I. INTRODUCTION

Mathematically, optical dark spatial solitons (DSSs) are exact solutions of the one-dimensional nonlinear Schrödinger equation (NLSE) for negative nonlinearity and nonvanishing boundary conditions [1]. Physically, they form on background beams of finite width as self-supported intensity dips due to the counterbalance between beam self-defocusing and diffraction. The required negative nonlinearity of the medium causes an inevitable reduction of the beam intensity. Losses, saturation and high transverse dimensionality result in nonintegrable model equations. Despite certain adiabatic relaxation characteristics, the solitary solutions of these equations have a large number of characteristics [2] in common with the soliton solution of the one-dimensional NLSE and are widely denoted by the term “dark soliton”. DSSs are generated as dark stripes [3,4], whereas the only known truly two-dimensional optical DSS is the optical vortex soliton (OVS) [5]. Characteristic of the phase portraits of these beams are a 1D π -phase jump and an on-axis 2π helical phase ramp, also denoted as edge-phase and screw-phase dislocations, respectively.

Optical ring dark solitary waves (RDSWs) were first introduced by Kivshar and Yang [6]. Their evolution was studied in the frame of the adiabatic approximation of perturbation theory. The quasi-one-dimensional treatment allowed the authors to obtain an expression for the RDSW's transverse velocity dR/dz as a function of the ring radius and the contrast. In addition, a linear stability analysis was performed. The authors showed that in the small-amplitude limit these ring dark waves are described by the cylindrical Korteweg-de Vries equation, which has ring soliton solutions [6]. Recently, Frantzeskakis and Malomed derived new equations of evolution for small-amplitude solitary waves on

a finite background [7] by means of a multiscale expansion method applied to the generalized cylindrical NLSE. Their long-wave solitary solutions propagate “on top” of the continuous-wave solution (i.e. on the background) as a dark perturbation in Kerr defocusing media. Depending on the background beam intensity, they can appear both dark and anti-dark for Kerr-like saturable defocusing nonlinearity.

The RDSWs may turn out to be of practical interest because of their ability to induce waveguides in which multiple signal beams could be guided parallel [8]. This requires detailed analysis of the dynamics of these solitary structures. The first experimental generation of optical RDSWs [9] was conducted with pure amplitude modulation in front of the nonlinear medium (reflective micrometer-sized dots illuminated by the background beam). Under such conditions, pairs of phases oppositely shifted by about $\pi/2$ were measured in each diametrical slice of the RDSWs [10]. In a subsequent experiment [11], RDSWs were generated from odd initial conditions by using binary computer-generated holograms (CGHs) [12]. Inside a circle the phase was shifted by π vs. the outlying area by shifting the photolithographically produced interference lines by half a grating period. In both experiments the phase profiles were measured by using the multiple-frame interferometric technique for optical wavefront reconstruction [13]. It was found that along the NLM the transverse velocity of the RDSWs born from even initial conditions is higher than that of the odd ones. Numerical simulations have shown that, besides the ring radius [6], the transverse velocity of the RDSW can be effectively controlled by initial phase modulation of the background beam (inside, outside or on both sides of the phase dislocation) or by nonlinear interaction with a second coaxial dark formation (RDSW or OVS) [14]. In saturable media, the RDSW's transverse velocity is

lower than that in Kerr NLM. At high saturation levels, in formal contradiction to but in actual agreement with the one-dimensional case, decay of the dark rings into a loop of optical vortices of alternate helicities should be expected [15].

We have measured experimentally the dynamics of ring dark solitary waves generated by different methods and compared those results with the predictions of the analytical method and numerical data. In particular, we analyzed the non-monotonic transverse velocity of RDSWs vs. background beam intensity in saturable NLM. The RDSWs are generated in the +1 and -1 diffraction order of the background beams. Comparative numerical simulations that account for the estimated contrast of the RDSWs and medium saturation are carried out. An intentional reduction of the magnitude of the phase shift encoded in the CGHs was found to have a substantial influence on the dark ring radii and the contrast at the entrance of the NLM. The differences in the nonlinear evolution of the RDSWs enable us to verify qualitatively the analytical result of Kivshar and Yang (see Eqs. 6 and 7 in Ref. [6]).

II. RDSW TRANSVERSE VELOCITY VS. INTENSITY

The experimental arrangement is shown in Fig. 1a. In order to obtain a dark ring of a desired radius and a phase jump of a certain magnitude, a single-line Ar^+ -laser ($\lambda = 488nm$) is used to reconstruct the respective CGH. The latter are produced photolithographically with a grating period of $18\mu m$ and ensure a diffraction efficiency of nearly 10% in first order. The nonlinear medium is ethylene glycol dyed with DODCI (Lambdachrome). The background beam, diffracted in first order with the dark ring nested in, is transmitted through a slit placed about 15 cm behind the CGH and is gently focused on the entrance of the NLM. After passing the desired nonlinear propagation path length (0.5cm to 8.5cm) the dark beam is partially reflected by a prism immersed in the liquid and is projected directly on a co-moving CCD array with a resolution of $13\mu m$. Alternatively, the dark beam can be recorded at the exit of the NLM. For further evaluation the images are stored by an image-capturing card.

The data presented in this section refer to an absorption of $\alpha = 0.107cm^{-1}$ at $\lambda = 488nm$. In a calibration measurement we generated a 1D DSS by using a CGH of the respective type. The soliton constant Ia^2 (i.e. the product of the background-beam intensity I and the square of the dark beam width a measured at the $1/e^2$ -level) is found to reach its asymptotically constant value for input powers $P_{sol}^{1D} \approx 90mW$ (Fig. 1b, dashed curve). Since the saturation of the (thermal) nonlinearity is expected to have important consequences on the RDSW's nonlinear dynamics [16], we realized a background-beam

self-bending scheme similar to that used in [17]. The required asymmetry is introduced by tilting the prism immersed in the NLM. This results in different propagation path lengths for different parts of the beam. The strength of the self-bending effect (Fig. 1b, solid curve) measured in the near field gives an estimated saturation power $P_{sat} \approx 35mW$. The choice of a saturation model for absorptive nonlocal nonlinearity is not trivial [18]. Here we use a sigmoidal fit of the type $f(I) \sim I/(1 + I/I_{sat})^3$.

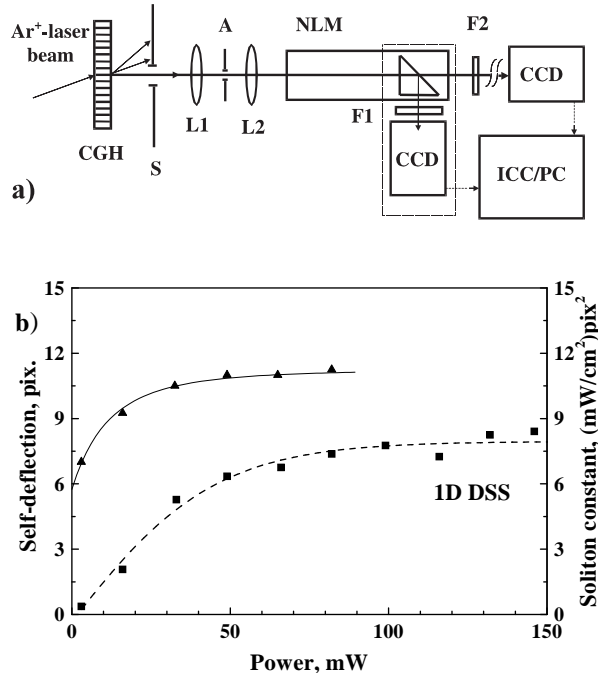


FIG. 1. **a)** Experimental setup: (CGH - computer-generated hologram, S - slit, A - aperture, L1 and L2 - AR-coated lenses ($f = 80mm$), NLM - nonlinear medium (ethylene glycol dyed with DODCI), F1, F2 - filter sets, CCD - charge-coupled device camera with $13\mu m$ resolution, ICC/PC - personal computer equipped with an image-capturing card). **b)** Power dependences of the background-beam self-deflection (triangles) and of the quantity Ia^2 (squares) indicating $P_{sat} \approx 35mW$ and $P_{sol}^{1D} \approx 90mW$. Solid (dashed) curve - sigmoidal fits.

When a RDSW is generated by pure amplitude modulation of the background beam at the entrance of the NLM, its transverse velocity increases monotonically with the intensity (up to $2.5P_{sol}^{1D}$; see Fig. 7 in Ref. [9]). By using the CGH of a black ring (with a phase jump of π), we observe a non-monotonic change of the ring radius vs. background beam power for a nonlinear propagation length of $z = 8.5cm$ (Fig. 2a). The corresponding data for the contrast of the RDSW $A^2 = (I_0 - I_{min})/I_0$ show reversed non-monotonic behaviour (Fig. 2b, solid curve). Generally, this is consistent with physical intuition and the theory [16] that the smaller the ring, the darker the solitary wave and the higher the total phase shift. As will be discussed later (see Fig. 4, the region on the left-hand

side of the vertical dashed line), the dark rings initially generated with a π -phase shift (“black”) become wider by diffraction and thus arrive as “dark-grey” at the entrance of the NLM. In our case the contrast is lowered to $A^2 = 0.88$ (see Fig. 2b). We measured the change of the RDSW’s radius at $z = 8.5\text{cm}$ as a function of the laser power. An evident minimum is observed for a power slightly below P_{sol}^{1D} . For this value the ring contrast is highest. Further insight can be gained by evaluating the analytical results for the phase of the solitary wave in the models of competing cubic-quintic and threshold nonlinearities (see Eqs. 6-9 in Ref. [16]). With the data for A^2 , both models show well-pronounced minima in the RDSW transverse velocity for powers slightly lower than P_{sol}^{1D} (Fig. 2, dashed curve). It should be noted that the experimental data in Fig. 2 were obtained by compensating losses during the propagation with an appropriate change of the input power. However, even for fixed input power the RDSW changes its transverse velocity along the medium. In that sense Fig. 2a presents the effect of the enhancement of the phase shift and the contrast of the RDSW by saturating the nonlinearity in an integral form. This result, however, does not explain why in our previous experiments only a monotonic increase of the RDSW radii was observed [9].

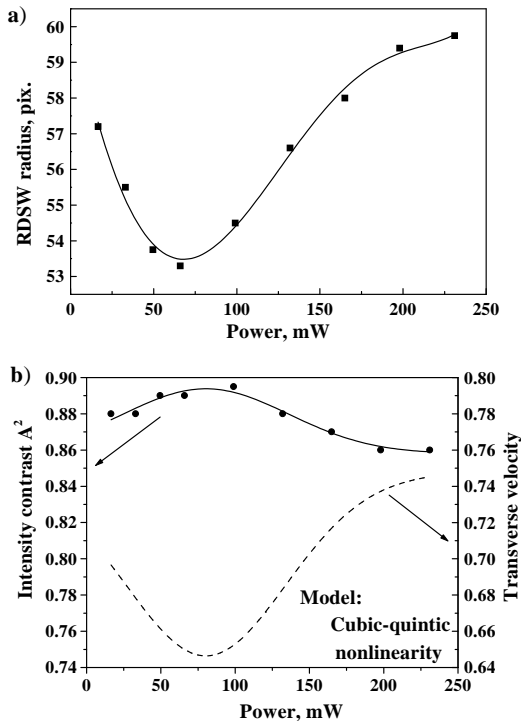


FIG. 2. **a)** Power dependence of the RDSW radius after a nonlinear propagation path length $z = 8.5\text{cm}$. **b)** Power dependence of the RDSW contrast (dots) and estimated transverse velocity (dashed curve) for saturable cubic-quintic nonlinearity. See text for details.

In order to explain this discrepancy we look at the

evolution of the RDSW before it enters the NLM. Numerical simulations are carried out for the evolution of “grey” solitary waves with initial radii $R_0 = R(z = 0)$ twice as large as the ring width $r_0 = r(z = 0)$. The numerical procedure used to solve the 2D NLSE is based on the beam propagation method over a 1024×1024 grid. In agreement with our measurement, initially “black” rings generated by CGHs become “grey” after passing four Rayleigh diffraction lengths $L_{Diff} = kr_0^2$ and reach the estimated contrast $A^2 = 0.88$. The evolution of the RDSW’s radius for different intensities is calculated for up to 10 nonlinear lengths ($L_{NL} = (k|n_2|I_0)^{-1}$, k is the wavenumber, and $|n_2|I_0$ the nonlinear refractive index correction). The behaviour of the RDSW radius in the NLM can be summarized as follows:

- i) For a fixed input intensity in the range of $(0.2 - 2.2)I_{sol}^{1D}$ all RDSWs have their minimal ring radius for propagation distances between $1.5L_{NL}$ and $3L_{NL}$.
- ii) For nonlinear propagation distances shorter than $2L_{NL}$ the grey rings monotonically reduce their radii for increasing intensity (Fig. 3, lowest box).
- iii) For long propagation distances ($> 6L_{NL}$) this tendency is reversed (Fig. 3, upper box).
- iv) In between, the radius of the RDSW as a function of the intensity shows a characteristic minimum around $4.5L_{NL}$ (Fig. 3, middle box). This propagation distance is in reasonable agreement with the NLM length of 8.5cm corresponding to $4L_{NL}$, for which Fig. 2 is obtained.

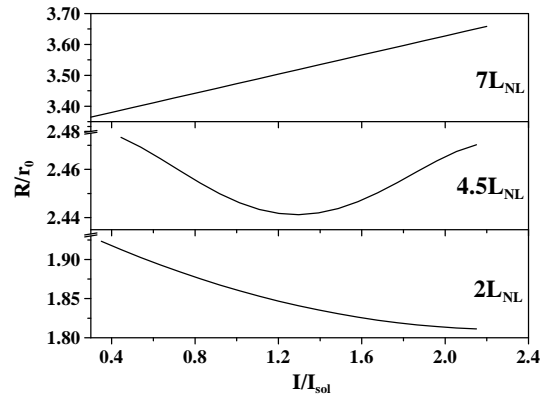


FIG. 3. RDSW radius vs. normalized background-beam intensity at three characteristic nonlinear propagation distances. Model parameters: $R_0/r_0 = 2$, $A^2 = 0.88$, $s = 0.4$.

Generally, we found qualitative confirmation of the existence of a minimal radius R_{min} of the RDSW, which depends on the initial contrast A^2 [6,16]. The evolution of the contrast itself is strongly influenced by the saturation of the nonlinearity. In view of the above it is interesting to recall the observation which we made when modeling the decay of multiple-charged OVSs under radial perturbations [19]: The small-amplitude even-phase initial conditions for perturbation and the saturation of the nonlinearity resulted in a negative transverse velocity of the rings. Their contrast was found to increase with

decreasing radius and the radial phase variation reached a maximum of 0.75π at $5L_{NL}$. The initially decaying and still strongly overlapping optical vortices partially recovered their multiple-charged state (Fig. 7 in Ref. [19]). Periodic sign changes in the transverse velocity of the dark rings in the propagation direction were observed in the simulations up to $10L_{NL}$ with a period of approximately $2L_{NL}$.

III. RDSW TRANSVERSE DYNAMICS VS. INITIAL PHASE SHIFT

It should be pointed out that initially “black” RDSWs with high transverse dynamics are not likely to be present in a real experiment, at least when generated by holograms. The reason lies in the necessity to select one of the diffracted beams, which requires a certain free-space propagation. After some diffraction is “accumulated”, the dark rings with small radii spread out substantially and their contrast decreases. Dark rings with large radii are less affected and they evolve more slowly inside the NLM. Figure 4 is intended to visualize this before and inside the NLM. The coordinate $z = 0$ is fixed on the nonlinear interface. Solid and dashed lines correspond to Kerr and saturable Kerr nonlinearity ($s = I/I_{sat} = 0.4$). The simulation presented is carried out for $I = I_{sol}^{1D}$ and for an initial phase jump of π , which will be flattened in the course of propagation. Generally, the saturation of the nonlinearity leads to a reduction of the dynamics of the RDSW. For our further considerations it is important to note that there is no difference whether the phase inside the ring Φ_{in} is bigger or lower than the phase Φ_{out} outside the ring, provided $\Delta\Phi = |\Phi_{in} - \Phi_{out}| = \pi$. Equivalently, there should be no difference in the transverse dynamics of the RDSWs generated by the +1st and -1st diffraction order beam when a phase jump of π is encoded in the CGHs. This was carefully proved by numerical simulations and experimentally.

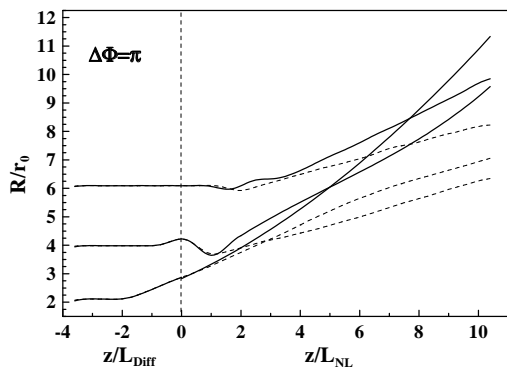


FIG. 4. Diffraction-governed evolution of odd RDSWs with initial π -phase jumps over 4 Rayleigh diffraction lengths followed by nonlinear propagation in a Kerr (solid curves) and saturable Kerr-like medium (dashed curves; $s = 0.4$). $I = I_{sol}^{1D}$. Vertical dashed line - the nonlinear interface.

A. Linear evolution for $|\Delta\Phi| < \pi$

The situation changes when we produce dark ring waves encoded on CGHs with phase shifts smaller than π . Unfortunately, in binary CGHs only π/N steps are possible, where one grating period consists of $2N$ elementary stripes. In our case $N = 3$ and the grey rings are designed for $|\Delta\Phi| = 2\pi/3$. The beam of a single-mode He-Ne laser is expanded 3.5 times and reproduces the respective CGH. By means of a lens ($f = 4cm$) the beam transmitted directly and the ± 1 st order diffracted beams are imaged on a screen located about $100cm$ behind. By varying the lens position we are able to follow the dark ring evolution. Figure 5a shows the images of the still overlapping first-order diffracted beams, which interfere with the zeroth order one. It can be seen clearly that the rings with $|\Delta\Phi| = 2\pi/3$ have smaller (larger) radius than each of the dark rings with an initial phase shift $|\Delta\Phi| = \pi$.

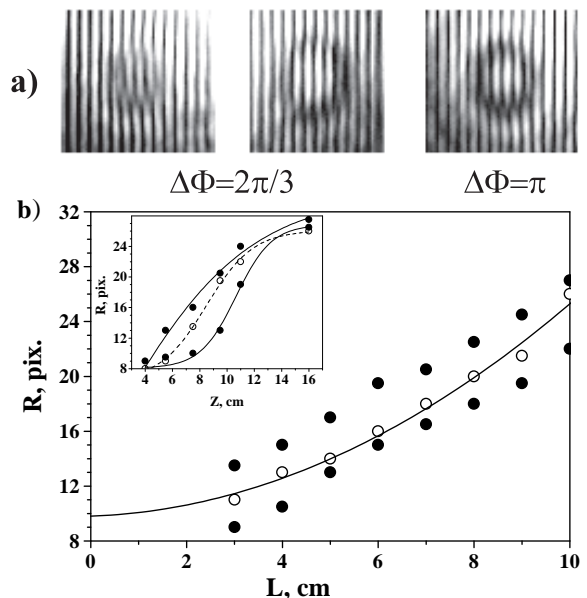


FIG. 5. Linear propagation of ring dark beams: **a)** Interference patterns indicating different transverse velocities of free-propagating, initially grey ($|\Delta\Phi| = 2\pi/3$) and black ($|\Delta\Phi| = \pi$) ring dark beams at $L = 5.5cm$. **b)** Host graph: ring radii vs. CGH-to-CCD-array distance L . Inset: the same vs. lens-to-CGH-distance. Dots - ± 1 st diffraction order beams, blank circles - initially black dark rings. See text for details.

The ring radii observed for lens positions from $4cm$ to $16cm$ are shown in the inset of Fig. 5b. In order to get better spatial resolution, the measurement was repeated with a CCD array illuminated directly after the CGH (Fig. 5b). Blank circles denote the dark ring radii for $|\Delta\Phi| = \pi$, the solid circles refer to the ring with encoded phase jump $|\Delta\Phi| = 2\pi/3$. Note that in the two graphs of Fig. 5b the ring radius R is denoted in CCD-camera pix-

els, but these units are not directly comparable because of the different focusing conditions. On the CGHs the ring radius is encoded in 20 pix. (i.e. $R_0 = 60\mu m$). It is easy to understand the observed differences: The diffraction tends to broaden the dark rings and flatten the phase jumps. As a result, for $\Phi_{in} < \Phi_{out}$ an effective concave phasefront is formed which “focuses” the dark ring. In the other diffraction order Φ_{out} appears to be bigger than Φ_{in} . The phase change induced by the diffraction results in an effective convex phasefront that increases the dark ring radius. For $|\Delta\Phi| = \pi$, the diffraction influences both first-order beams in the same way, but more weakly.

B. Nonlinear evolution of initially grey RDSWs

Although the nonlinear regime was analytically analyzed by Kivshar and Yang [6], to the best of our knowledge it has not been investigated experimentally. The basic results (Eqs. 5-7 in Ref [6]) can be summarized as follows:

- i) For each RDSW there is a minimum ring radius R_{min} for which the RDSW has its highest contrast.
- ii) Depending on the initial value of the phase jump, the RDSW either collapses along the NLM to reach R_{min} and diverge monotonically thereafter, or it diverges monotonically from the beginning.

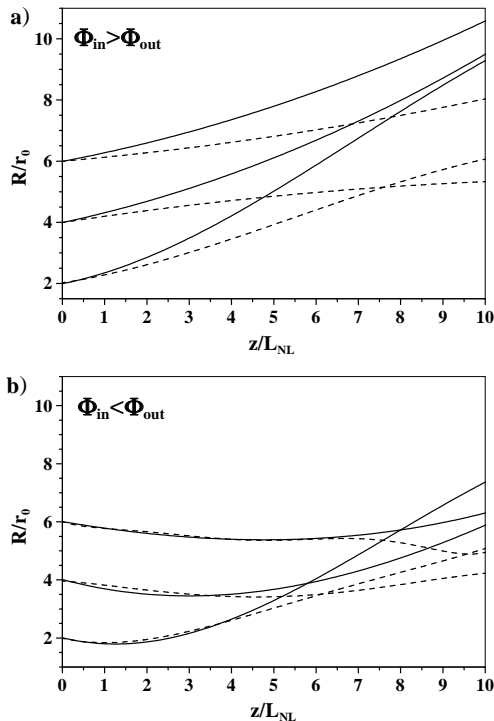


FIG. 6. Nonlinear evolution of initially grey RDSWs in a Kerr (solid curves) and saturable Kerr-like medium (dashed; $s = 0.4$) for positive (a) and negative (b) phase shift $\Delta\Phi = \Phi_{in} - \Phi_{out}$. The model parameters correspond to $A^2 = 0.88$ (i.e. to $|\Delta\Phi| = 0.837\pi$) and $I = I_{sol}^{1D}$.

Figure 6 is intended to clarify these conclusions. We solved the NLSE numerically by keeping the following parameters close to the experimental values: RDSW radii ($(R/r)|_{z=0} = 2, 4, \text{ and } 6$), background-beam intensity ($I = I_{sol}^{1D}$), initial contrast $A^2 = 0.88$, phase jump $|\Delta\Phi| = 0.837\pi$, and saturation of the nonlinearity $s = 0.4$. In Fig. 6a the corresponding results for the case of a higher phase inside the rings ($\Phi_{in} > \Phi_{out}$) are presented. In this case, the RDSWs start diverging immediately after entering the NLM. The data shown in Fig. 6b refer to the case of a lower phase inside the dark ring and higher phase outside ($\Phi_{in} < \Phi_{out}$). The effective concave wavefront forces the RDSWs to collapse to a minimum ring diameter. Thereafter they start to broaden faster. The main tendency, that the broader the RDSW initially is, the longer the nonlinear propagation needed to reach R_{min} will be, is well expressed. The other general tendency, that the smaller the RDSW diameter is, the higher its transverse dynamics is, can also be clearly seen.

Both tendencies and the influence of the saturation seem to be understood theoretically, but still need experimental confirmation. We performed additional measurements with the experimental setup shown in Fig. 1, in which the telescope is replaced by a single lens ($f = 12cm$) in order to focus the beams near the entrance of the NLM. Moderate and strong saturation s can be achieved by raising the absorption α to $0.2cm^{-1}$ ($P_{sol}^{1D} = 25mW$; $P_{sat} = 40mW$; $s = 0.6$) and $0.4cm^{-1}$ ($P_{sol}^{1D} = 20mW$; $P_{sat} = 14(\pm 5)mW$; $s \approx 1.4$). In order to keep the conditions for both first-order beams as similar as possible, the beam transmitted directly was blocked at the entrance of the NLM and both $\pm 1st$ order beams were recorded simultaneously. Unfortunately, due to the interaction of the two background beams, the interaction-free nonlinear propagation path length is limited. The results of the measurements are shown in Fig. 7a for moderate and high saturation (host graph and inset, respectively). Blank circles denote “black” RDSWs radii, solid ones RDSW radii for $\Delta\Phi = \pm 2\pi/3$. The best results for moderate saturation are achieved with CGHs containing phase dislocations with radii of $R = 30\mu m$. For high saturation, rings with dislocation radii of $60\mu m$ are used. As seen, after some $5mm$ of nonlinear propagation the “grey” RDSWs reach R_{min} and diverge monotonically afterwards. The beam of the other diffraction order and the RDSW generated for $|\Delta\Phi| = \pi$ start diverging from the beginning. The interpolated curves in the figure are intended to guide the eye. The interpolated curves for $z < 2mm$ and $z > 17mm$ are not shown for an obvious physical reason: As mentioned, the grey RDSWs do not enter the NLM with equal radii and equal (absolute) phase shifts. For larger propagation distances, the saturation-like behaviour is caused mainly by interaction with the second co-propagating beam. The reduced transverse velocities of the RDSWs for higher saturation are also strongly pronounced. The grey-scale images in Fig. 7b show the RDSWs at $z = 2mm$ and $8mm$ inside

the NLM.

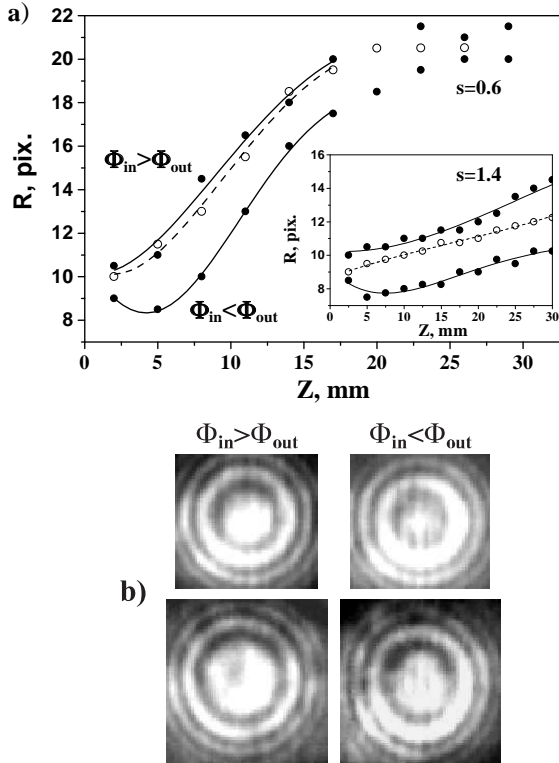


FIG. 7. Nonlinear propagation of RDSWs: **a)** Evolution of the RDSW radii along the nonlinear medium at moderate (host graph, $s = 0.6$) and high saturation (inset, $s \approx 1.4$). Solid and blank circles - initially grey ($|\Delta\Phi| = 2\pi/3$) and black ($|\Delta\Phi| = \pi$) RDSWs, respectively. **b)** Grey-scale images of RDSWs at $z = 2\text{mm}$ (upper row) and 8mm (lower row) in a moderately saturated NLM.

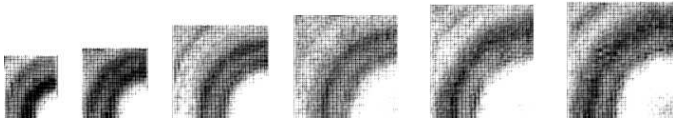


FIG. 8. Gray-scale images showing the development of an internal substructure of a RDSW ($R_0 = 90\mu\text{m}$) at moderate saturation. Left to right: $z = 2, 5, 8, 11, 14,$ and 17mm .

By evaluating the data corresponding to the largest RDSWs in our experiment ($R = 90\mu\text{m}$) we observed internal ring splitting for moderate saturation (Fig. 8). Despite their large radii, these RDSWs have non-zero transverse velocity. They broaden and flatten due to the saturation (see Fig. 8, frame at $z = 2\text{mm}$) while evolving into grey rings. It seems that such a grey ring can serve as a background on which two coaxial rings can form, subsequently narrow and thus get a high modulation depth for increased propagation distance (Fig. 8, frames at $z = 5, 8, 11, 14,$ and 17mm). The mechanism for their formation includes effects from increasing a phase shift and decreasing a transverse velocity due to the saturation of the nonlinearity [16], as well as repulsion between op-

posite quasi-2D phase dislocations. The relation of these coaxial rings to the small-amplitude dark solitary waves described by Frantzeskakis and Malomed [7] should be clarified.

IV. CONCLUSION

It is worth noting that it is difficult (if possible at all) to ensure perfect odd initial conditions (radial phase jumps equal to π and contrast equal to unity) for the generation of RDSWs in cubic nonlinear media. When such a phase jump is encoded in a CGH, there is no difference between the evolution of the two beams in first diffraction order. This changes gradually for smaller phase jumps. In qualitative agreement with the theory [6] we presented evidence of the monotonic increase of the dark ring radius for $\Phi_{in} > \Phi_{out}$ and the corresponding non-monotonicity in the opposite case. For grey initial conditions and saturation of the nonlinearity we found characteristic regions for the dependence of the RDSW radius on the background-beam intensity. The radius can increase, decrease monotonically or go through a minimum. The results presented are in qualitative agreement with the analytical ones regarding the phase of the solitary wave in the presence of saturation [16].

ACKNOWLEDGMENTS

The authors are pleased to acknowledge highly useful discussions with Prof. Yu. Kivshar and his suggestions for improving the manuscript. A. D. would like to thank the Alexander von Humboldt Foundation for the award of a fellowship and the opportunity to work in the stimulating atmosphere of Max-Planck-Institut für Quantenoptik (Garching, Germany). This work was also supported by the National Science Foundation of Bulgaria and by the Science Fund of Sofia University.

- [1] V. Zakharov, A. Shabat, Zh. Eksp. Teor. Fiz. **64**, 1627 (1973); in Russian: Sov. Phys. JETP **37**, 823 (1973).
- [2] Yu. S. Kivshar, B. Luther-Davies, Physics Reports **289**, 81 (1997).
- [3] G. A. Swartzlander, Jr., D. R. Andersen, J. J. Regan, H. Yin, and A. E. Kaplan, Phys. Rev. Lett. **66**, 1583 (1991).
- [4] B. Luther Davies, Y. Xiaping, Opt. Lett. **17**, 496 (1992).
- [5] G. A. Swartzlander, Jr., C. T. Law, Phys. Rev. Lett. **69**, 2503 (1992); C. T. Law, G. A. Swartzlander, Jr., Opt. Lett. **18**, 586 (1993); V. Tikhonenko, Yu. S. Kivshar, V. V. Steblina, and A. A. Zozulya, J. Opt. Soc. Am. **B 15**, 79 (1998).

- [6] Yu. S. Kivshar, X. Yang, Phys. Rev. **E 50**, R40-R43 (1994); Chaos, Solitons & Fractals **4**, 1745 (1994).
- [7] D. J. Frantzeskakis, B. A. Malomed, Phys. Lett. **A 264**, 179 (1999).
- [8] A. Dreischuh, V. Kamenov, and S. Dinev, Appl. Phys. **B 63**, 145 (1996).
- [9] S. Balushev, A. Dreischuh, I. Velchev, S. Dinev, and O. Marazov, Appl. Phys. **B 61**, 121 (1995); Phys. Rev. **E 52**, 5517 (1995).
- [10] A. Dreischuh, W. Fließner, I. Velchev, S. Dinev, and L. Windholz, Appl. Phys. **B 62**, 139 (1996).
- [11] D. Neshev, A. Dreischuh, V. Kamenov, I. Stefanov, S. Dinev, W. Fließner, and L. Windholz, Appl. Phys. **B 64**, 429 (1997).
- [12] W.-H. Lee, Prog. Optics **XVI**, 119 (1978).
- [13] C. Creath: in *Temporal Phase Measurement Methods in Interferogram Analysis*, edited by D. Robinson and G. Reid (Inst. of Physics, Bristol, 1993) pp. 94-140.
- [14] V. Kamenov, A. Dreischuh, Physica Scripta **55**, 68 (1997).
- [15] E. D. Eugenieva, A. A. Dreischuh, Physica Scripta **58**, 481 (1998).
- [16] W. Krolikowski, N. Akhmediev, and B. Luther-Davies, Phys. Rev. **E 48**, 3980 (1993).
- [17] A. E. Kaplan, JETP Lett. **9**, 33 (1969); M. S. Borodin, A. M. Kamuz, JETP Lett. **9**, 351 (1969).
- [18] V. Tikhonenko, J. Christou, B. Luther-Davies, and Yu. S. Kivshar, Opt. Lett. **21**, 1129 (1996).
- [19] A. Dreischuh, G. G. Paulus, F. Zacher, F. Grasbon, D. Neshev, and H. Walther, Phys. Rev. **E 60**, 7518 (1999).